Recovery of the parameters of cancellous bone by inversion of effective velocities, and transmission and reflection coefficients

James L. Buchanan
Mathematics Department
United States Naval Academy
Annapolis, MD 21402, USA
jlb@usna.edu

Robert P. Gilbert
Department of Mathematical Sciences
University of Delaware
Newark, DE 19711, USA
gilbert@math.udel.edu

Miao-jung Y. Ou
Department of Mathematical Sciences
University of Delaware
Newark, DE 19711, USA
mou@math.udel.edu

September 3, 2011

Abstract

Estimating the parameters of an elastic or poroelastic medium from reflected or transmitted acoustic data is an important, but difficult problem. Use of the Nelder-Mead simplex method to minimize an objective function measuring the discrepancy between some observable and its value calculated from a model for a trial set of parameters has been tried by several authors. In this article the difficulty with this direct approach, which is the existence of numerous local minima of the objective function, is documented for the *in vitro* experiment in which a specimen in a water tank is subject to an ultrasonic pulse. An indirect approach, based on numerical solution of the equations for a set "effective" velocities and transmission coefficients, is then observed empirically to ameliorate the difficulties posed by the direct approach.

1 Introduction

Cancellous bone is a two component material consisting of a calcified bone matrix, composed of rod shaped trabeculae, with interstitial fatty marrow. The bone disease osteoporosis is the result of the thinning of the trabecular matrix. As cancellous bone is poroelastic, Biot's mathematical model [Biot, 1956a], [Biot, 1956b], [Biot, 1962a], [Biot, 1962b] of a poroelastic medium is applicable. Early attempts to model observations using the Biot model met with mixed success. The article of [Haire & Langton, 1999] provides a good review of the attempts to apply the Biot model to cancellous bone prior to the year 2000.

One means of exploring the structure of cancellous bone is the *in vitro* experiment, in which a small rectangular or cylindrical element of excised bone placed in water tank is subjected to an ultrasonic pulse. Such an experiment conducted by [Hosokawa & Otani, 1997], led to the observation of two images of the incident pulse arriving at the receiver at different times. The existence of two compressional waves of different velocities is a prediction of the Biot model for an isotropic medium. Subsequently [Fellah *et al.* , 2004] and [Sebaa *et al.* , 2006] showed that observed transmitted waveforms were in good agreement with the predictions of the modification of the Biot model due to [Johnson *et al.* , 1987].

Estimating the parameters of an elastic or poroelastic medium from reflected or transmitted acoustic data is an important, but difficult problem. A good discussion of the possible approaches and difficulties in the recovery of bathymetric and bottom parameters in ocean acoustics can be found in [Gerstoft, 1994]. The problem of recovering the parameters of cancellous bone has been explored by [Buchanan *et al.* , 2002],[Buchanan *et al.* , 2004],[Buchanan & Gilbert, 2007], and [Sebaa *et al.* , 2006]. The approach in these articles was direct use of the Nelder-Mead simplex method to minimize an objective function measuring the discrepancy between some observable and its value calculated from a model for a trial set of parameters. In this article the difficulty with the direct approach, which is the existence of numerous local minima of the objective function, is documented for the *in vitro* experiment. An alternative approach, taken for instance by [Chotiros, 2002] in finding the Biot parameters for water-saturated sands, is numerical solution of a system of equations. This requires an equal number of observables and unknowns. This approach, based on numerical solution of the equations for a set "effective" velocities and transmission coefficients, will be considered in this article.

2 The mathematical model

A water-tank experiment similar as to those conducted by [Hosokawa & Otani, 1997], [Fellah *et al.* , 2004] and [Sebaa *et al.* , 2006] is illustrated in Figure 1 and described mathematically as follows. Consider a poroelastic segment $\mathcal{B}$ of length L, lying along the x-axis abutted on the left by a fluid layer $\mathcal{F}_L$ containing a point source transmitter/receiver at $x = x_T$ and on the right by a fluid layer $\mathcal{F}_R$ containing a receiver at $x = x_R$. Letting the left edge of $\mathcal{B}$ be at $x = 0$, the

Parameter	Symbol	Units
Porosity	β	
Asymptotic tortuosity	α_∞	
Viscous characteristic length	Λ	m
Permeability	k	m^2
Fluid density	ρ_f	$\mathrm{kg}\cdot\mathrm{m}^{-3}$
Fluid bulk modulus	K_f	Pa
Fluid viscosity	η	$\mathrm{kg}\cdot(\mathrm{m}\cdot\mathrm{s})^{-1}$
Frame material density	ρ_s	$\mathrm{kg}\cdot\mathrm{m}^{-3}$
Frame material bulk modulus	K_s	Pa

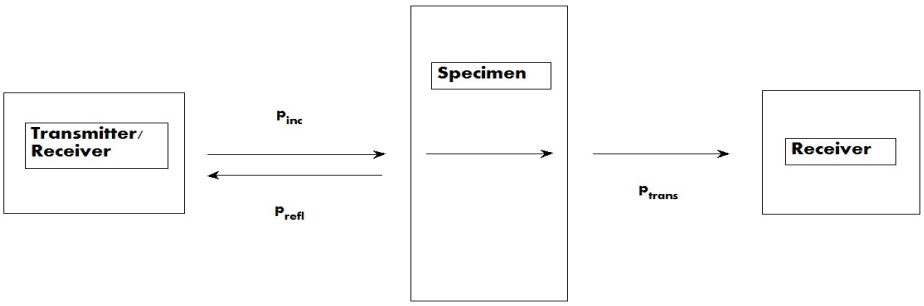

Figure 1: Schematic of a water tank experiment.

partial differential equations governing pressure in the fluid regions are

$$\frac{\partial^2 p_L}{\partial x^2} - \frac{1}{c_L^2}\frac{\partial^2 p_L}{\partial t^2} = -f(t)\delta(x - x_T), -\infty < x < 0$$
$$\frac{\partial^2 p_R}{\partial x^2} - \frac{1}{c_R^2}\frac{\partial^2 p_R}{\partial t^2} = 0, L < x < \infty,$$

where c_L and c_R are the wave speeds in the left and right fluid regions. In this article the JKD modification of Biot's model of a poroelastic medium due to Johnson *et a*l. [Johnson *et al.* , 1987] is used to describe wave propagation in the poroelastic segment. The input parameters of this model are given in Table 1. In the JKD model tortuosity is dynamic, i.e. it varies with frequency ω

$$\alpha(\omega) = \alpha_\infty \left(1 + \frac{\eta\beta}{i\omega\alpha_\infty\rho_f k}\sqrt{1 + i\frac{4\alpha_\infty^2 k^2\rho_f\omega}{\eta\Lambda^2\beta^2}}\right).$$

The specific attenuation per cycle is asymptotically d/Λ where $d = \sqrt{2\eta/(\rho_f\omega)}$ is the width of the boundary layer to the frame in which vorticity is significant.

The governing partial differential equations in the poroelastic segment are

$$\begin{bmatrix} \frac{\partial^2 u}{\partial x^2} \\ \frac{\partial^2 U}{\partial x^2} \end{bmatrix} = \begin{bmatrix} P & Q \\ Q & R \end{bmatrix}^{-1} \begin{bmatrix} \rho_{11} & \rho_{12} \\ \rho_{12} & \rho_{22} \end{bmatrix} \begin{bmatrix} \frac{\partial^2 u}{\partial t^2} \\ \frac{\partial^2 U}{\partial t^2} \end{bmatrix}, 0 < x < L.$$

The quantities $u(x,t)$ and $U(x,t)$ track the motions of the frame and interstitial fluid respectively. The moduli P, Q, and R in the Biot model are calculated from the inputs in Table 1

$$\begin{aligned} P &:= \frac{(1-\beta)\left(1-\beta-\frac{K_b}{K_s}\right)K_s + \beta\frac{K_s}{K_f}K_b}{1-\beta-\frac{K_b}{K_s}+\beta\frac{K_s}{K_f}} + \frac{4}{3}G \\ Q &:= \frac{\left(1-\beta-\frac{K_b}{K_s}\right)\beta K_s}{1-\beta-\frac{K_b}{K_s}+\beta\frac{K_s}{K_f}} \\ R &:= \frac{\beta^2 K_s}{1-\beta-\frac{K_b}{K_s}+\beta\frac{K_s}{K_f}} \end{aligned}$$

All of the parameters in Table 1 are independent of frequency in the JKD model, and thus so are P, Q, and R. The high-frequency approximations to the mass-coupling coefficients

$$\begin{aligned} \rho_{11} &= (1-\beta)\rho_s + \beta\rho_f(\alpha(\omega)-1) \\ &\cong (1-\beta)\rho_s + \beta\rho_f(\alpha_\infty - 1) + \frac{Z}{\sqrt{i\omega}} \\ \rho_{12} &= -\beta\rho_f(\alpha(\omega)-1) \\ &\cong -\beta\rho_f(\alpha_\infty - 1) - \frac{Z}{\sqrt{i\omega}} \\ \rho_{22} &= \beta\alpha(\omega)\rho_f \\ &\cong \beta\alpha_\infty\rho_f + \frac{Z}{\sqrt{i\omega}} \end{aligned} \tag{1}$$

where

$$Z = \frac{2\beta\alpha_\infty}{\Lambda}\sqrt{\rho_f\eta}$$

are appropriate for an ultrasonic source. Thus at frequencies high enough for these approximations to be valid, the governing equations are independent of permeability. Figure 2 shows that for Sample M1F04 of Table 2 and permeabilities in the range $10^{-10} - 10^{-8}\,\mathrm{m}^2$ suggested in [McKelvie & Palmer, 1991], the high-frequency approximations in (1) are valid down to frequencies below 100 kHz.

In the two fluid segments displacement is related to fluid pressure by

$$\rho\frac{\partial^2 U}{\partial t^2} = -\frac{\partial p}{\partial x}$$

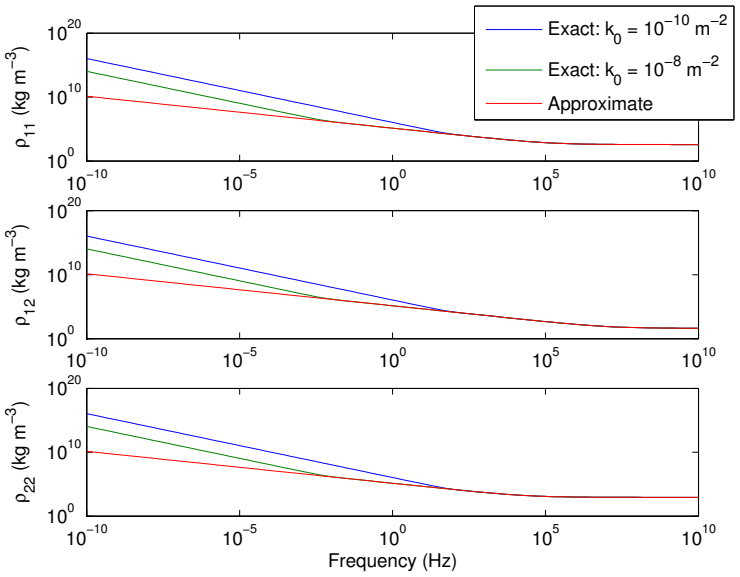

Figure 2: Comparison of the exact and approximate formulas for the density parameters given in (1) for two values of permeability k_0. The sample was M1F04 of Table 2.

where ρ is the fluid's density. Normal frame stress and pore fluid stress are related to the frame and fluid displacements by

$$\begin{aligned} \sigma_{xx} &= P\frac{\partial u}{\partial x} + Q\frac{\partial U}{\partial x} \\ \sigma_f &= Q\frac{\partial u}{\partial x} + R\frac{\partial U}{\partial x} \end{aligned} \tag{2}$$

respectively. Pore fluid pressure is related to pore fluid stress by $p_f = -\sigma_f/\beta$. At the fluid-poroelastic interface $x = 0$ continuity of total pressure, continuity of pore fluid pressure, and continuity of specific flux give

$$\begin{aligned} -p_L(0,t) &= \sigma_{xx}(0,t) + \sigma_f(0,t) \\ p_L(0,t) &= -\frac{\sigma_f(0,t)}{\beta} \\ \frac{\partial U_L}{\partial t}(0,t) &= \beta\frac{\partial U}{\partial t}(0,t) + (1-\beta)\,\frac{\partial u}{\partial t}(0,t). \end{aligned} \tag{3}$$

Comparable conditions are imposed at the other fluid-poroelastic interface $x = L$.

3 Solution by integral transform

Let $\hat{g}(s) = \mathcal{L}\{g(t)\} = \int_0^\infty e^{-st} g(t) dt$ denote the Laplace transform of a function g. The transformed problem is

$$\begin{aligned}
&\frac{\partial^2 \hat{p}_L}{\partial x^2} - \frac{s^2}{c_L^2}\hat{p}_L = -\hat{f}(s)\delta(x - x_T), -\infty < x < 0 \qquad (4)\\
&\begin{bmatrix} \frac{d^2\hat{u}}{dx^2} \\ \frac{d^2\hat{U}}{dx^2} \end{bmatrix} = s^2 \begin{bmatrix} P & Q \\ Q & R \end{bmatrix}^{-1} \begin{bmatrix} \rho_{11} & \rho_{12} \\ \rho_{12} & \rho_{22} \end{bmatrix} \begin{bmatrix} \hat{u} \\ \hat{U} \end{bmatrix}, 0 < x < L\\
&\frac{\partial^2 \hat{p}_R}{\partial x^2} - \frac{s^2}{c_R^2}\hat{p}_R = 0, L < x < \infty.
\end{aligned}$$

For all of the simulations presented in this article $s = i\omega$ sufficed.

The system of equations for the poroelastic segment in (4) can be written

$$\begin{pmatrix} \frac{d^2\hat{u}}{dx^2} \\ \frac{d^2\hat{U}}{dx^2} \end{pmatrix} = \left(\frac{s^2}{PR - Q^2}\right) \begin{pmatrix} R\rho_{11} - Q\rho_{12} & R\rho_{12} - Q\rho_{22} \\ -Q\rho_{11} + P\rho_{12} & -Q\rho_{12} + P\rho_{22} \end{pmatrix} \begin{pmatrix} \hat{u} \\ \hat{U} \end{pmatrix}.$$

In terms of the eigenvalues λ_j and corresponding eigenvectors $\mathbf{v}_j, j = 1, 2$, of the matrix on the right hand side the system becomes

$$\begin{pmatrix} \frac{d^2\hat{u}}{dx^2} \\ \frac{d^2\hat{U}}{dx^2} \end{pmatrix} = \frac{s^2}{PR - Q^2} \mathbf{V}\mathbf{\Delta}\mathbf{V}^{-1} \begin{pmatrix} \hat{u} \\ \hat{U} \end{pmatrix}$$

where

$$\mathbf{V} = \begin{pmatrix} \mathbf{v}_1 & \mathbf{v}_2 \end{pmatrix}, \mathbf{\Delta} = \begin{pmatrix} \lambda_1 & 0 \\ 0 & \lambda_2 \end{pmatrix}.$$

With

$$\begin{aligned}
b &:= -R\rho_{11} + 2Q\rho_{12} - P\rho_{22}\\
c &:= RP(\rho_{11}\rho_{22} - \rho_{12}^2) + Q^2(\rho_{12}^2 - \rho_{22}\rho_{11})
\end{aligned}$$

the eigenvalues are

$$\lambda_1 = \frac{-b - \sqrt{b^2 - 4c}}{2}, \lambda_2 = \frac{-b + \sqrt{b^2 - 4c}}{2}$$

with corresponding eigenvectors

$$\mathbf{v}_i = \begin{pmatrix} v_{i1} \\ v_{i2} \end{pmatrix} = \frac{1}{\sqrt{1 + \left(\frac{R\rho_{11} - Q\rho_{12} - \lambda_i}{Q\rho_{22} - R\rho_{12}}\right)^2}} \begin{pmatrix} 1 \\ \frac{R\rho_{11} - Q\rho_{12} - \lambda_i}{Q\rho_{22} - R\rho_{12}} \end{pmatrix}, i = 1, 2. \qquad (5)$$

The Biot theory predicts two compressional waves, a fast wave and a slow wave, with complex-valued velocities

$$c_F = \left(\frac{\lambda_1}{PR - Q^2}\right)^{-1/2}, c_S = \left(\frac{\lambda_2}{PR - Q^2}\right)^{-1/2}. \qquad (6)$$

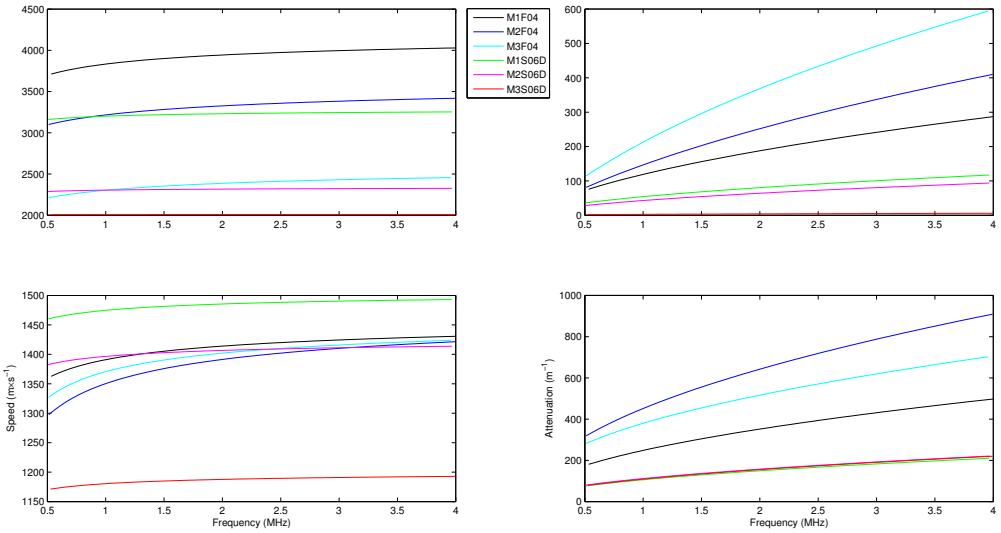

Figure 3: Fast (upper panes) and slow (lower panes) wave speeds and attenuations for the six parameter sets of Table 2.

From these the velocity and attenuation are calculated as

$$v_J = \frac{|c_J|^2}{\mathrm{Re}\, c_J}, a_J = \frac{\mathrm{Im}\, c_J}{|c_J|^2}, J = F, S. \tag{7}$$

Figure 3 shows fast and slow wave speeds and attenuations for the six sample of Table 2 below.

The solution to (4) has the form

$$\hat{p}_L = C_1 \exp(sx/c_L), -\infty < x < x_T \tag{8}$$
$$\hat{p}_L = C_2 \exp(-sx/c_L) + C_3 \exp(sx/c_L), x_T < x < 0$$
$$\hat{u} = C_4 v_{F1} \exp(-sx/c_F) + C_5 v_{F1} \exp(sx/c_F) + C_6 v_{S1} \exp(-sx/c_S) + C_7 v_{S1} \exp(sx/c_S), 0 < x < L$$
$$\hat{U} = C_4 v_{F2} \exp(-sx/c_F) + C_5 v_{F2} \exp(sx/c_F) + C_6 v_{S2} \exp(-sx/c_S) + C_7 v_{S2} \exp(sx/c_S), 0 < x < L$$
$$\hat{p}_R = C_8 \exp(-sx/c_R), L < x < \infty.$$

Here the notation $v_{Fj} = v_{1j}, v_{Sj} = v_{2j}, j = 1, 2$ has been adopted. The transformed jump conditions for the delta function

$$\hat{p}_L(x_T^+) - \hat{p}_L(x_T^-) = 0 \tag{9}$$
$$\frac{\partial \hat{p}_L}{\partial x}(x_T^+) - \frac{\partial \hat{p}_L}{\partial x}(x_T^-) = -\frac{\hat{f}}{c_L^2},$$

and the transforms of the three conditions (3) at the two fluid-poroelastic interfaces $x = 0, L$ yield a 8×8 linear system

$$A\boldsymbol{C} = \boldsymbol{b} \tag{10}$$

$$\boldsymbol{C} = \{C_j\}_{j=1}^{8}, \boldsymbol{b} = \left[0, -\frac{\hat{f}}{c_L^2}, 0, \ldots, 0\right]^T$$

for the coefficients in (8).

4 Simulated transmitted and reflected pressure waves

In order to study the feasibility of recovering some of the Biot-JKD parameters from experimentally measured reflected and transmitted pressure waves, it is necessary to simulate these observations. The incident pulse

$$f(t) = \exp\left(-\left(t - t_c\right)^2 / \Sigma\right) \sin \omega_0 t \tag{11}$$

with $f_0 = 2.25\,\mathrm{MHz}, \omega_0 = 2\pi f_0, t_0 = 1/f_0, \Sigma = t_0^2$ is used. Laplace and inverse Laplace transforms are approximated using the fast Fourier transform as described in [Buchanan *et al.* , 2011a], [Buchanan *et al.* , 2011b]. All instances of square roots of complex-valued quantities such as those in (1) and (5) were evaluated using MATLAB's *sqrt*, which takes the branch cut to be the positive real axis. Figure 4 shows the pressure wave incident on the left edge of the bone specimen and its spectral content for $t_c = 1.75t_0, 1.9t_0, 2.0t_0$. For purpose of computing inverse Laplace transforms frequency is restricted to the range $0.5 - 4\,\mathrm{MHz}$, since this encompasses the strongest portion of the spectrum of the incident pulse. Figure 2 suggests that the high-frequency JKD approximations (1) are valid in this range.

For simulations the parameters of Table 2 are used. The parameters for specimens M1F04-M3F04 were taken from [Fellah *et al.* , 2004] while M1S06D-M3S06D are the measured values of the drained specimens given in [Sebaa *et al.* , 2006]. In the experiments being simulated the interstitial fluid is the tank water hence $c_F = c_R = c_0$. The remaining parameters of Table 1, which are the same for all simulations, are $\rho_f = 1000\,\mathrm{kg \cdot m^{-3}}, K_f = 2.28 \times 10^9\,\mathrm{Pa}, \eta = 0.001\,\mathrm{kg \cdot (m \cdot s)^{-1}}$.

From (8) the received pulses at positions $x = x_T$ and $x = x_R$ are

$$p_L = \mathcal{L}^{-1}\left\{C_3 \exp(sx_T/c_0)\right\} = \mathcal{L}^{-1}\left\{\mathcal{R}_{\mathrm{Total}} \exp\left(-2sx_T/c_0\right) \frac{\hat{f}}{s}\right\} \tag{12}$$

$$p_R = \mathcal{L}^{-1}\left\{C_8 \exp(-sx_R/c_0)\right\} = \mathcal{L}^{-1}\left\{\mathcal{T}_{\mathrm{Total}} \exp\left(-s\left(-x_T/c_0 + (x_R - L)/c_0\right)\right) \frac{\hat{f}}{s}\right\}$$

where the reflection and transmission coefficients $\mathcal{R}_{\mathrm{Total}}$ and $\mathcal{T}_{\mathrm{Total}}$ are expressible in terms of the frequency-domain exponentials

$$e_1 = \exp\left(-sL/c_F\right), e_2 = \exp\left(-sL/c_S\right) \tag{13}$$

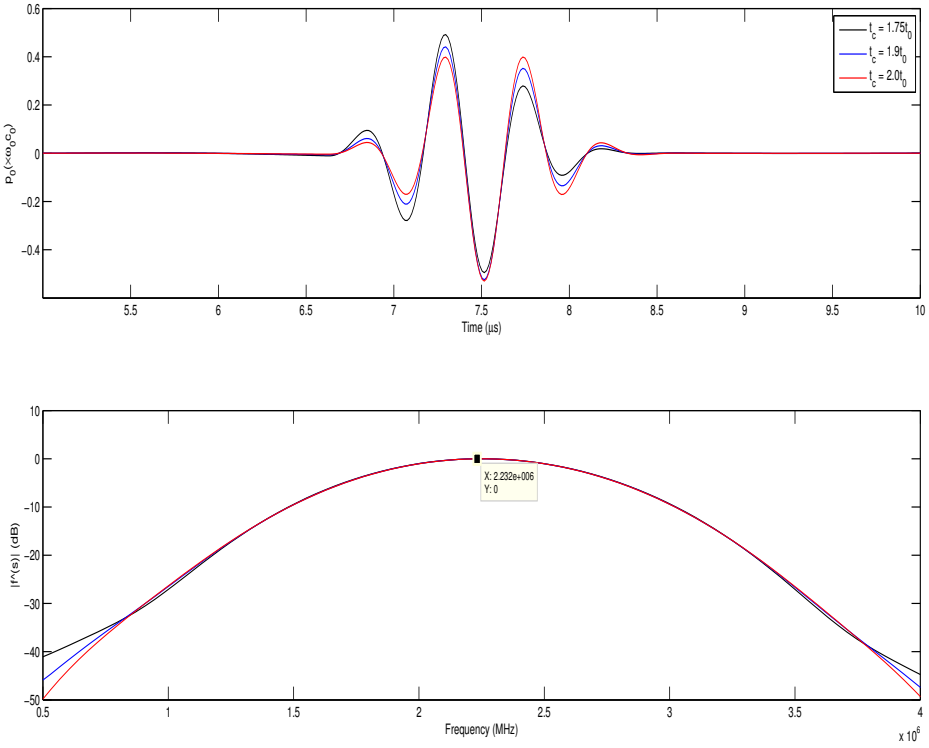

Figure 4: Top: Incident pulses travelling in the water to the left of the bone segment before first interaction with the bone for three values of the parameter t_c in (11). Bottom: Spectral content of the pulses.

	M1F04	M2F04	M3F04	M1S06D	M2S06D	M3S06D
β	0.83	0.77	0.88	0.71	0.75	0.55
α_∞	1.05	1.01	1.02	1.02	1.045	1.08
Λ	5.00E-06	2.70E-06	2.70E-06	1.04E-05	1.50E-05	1.95E-05
ρ_s	1960	1960	1960	1990	1990	1990
K_s	2.00E+10	2.00E+10	2.60E+10	1.08E+10	1.08E+10	1.08E+10
G	2.60E+09	1.70E+09	3.50E+08	1.77E+09	9.68E+08	1.07E+09
K_b	3.30E+09	4.00E+09	1.30E+09	4.08E+09	1.54E+09	1.49E+09

Table 2: JKD parameters for six specimens. M1F04-M3F04 are from [Fellah *et al.* , 2004] and M1S06-M3S06 are from [Sebaa *et al.* , 2006].

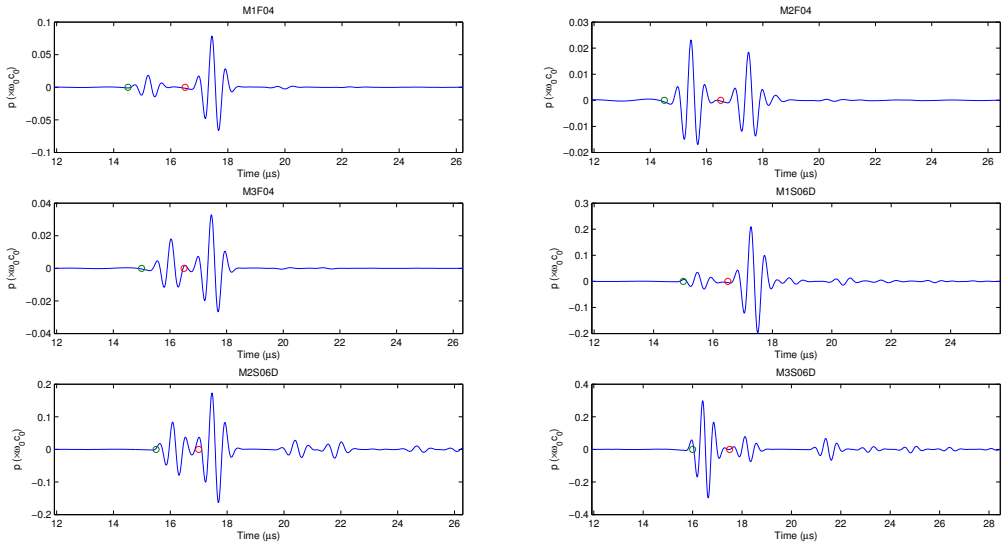

Figure 5: $L = 5\,\text{mm}$. Circles are the rough estimates of the arrival times of the fast and slow waves used in the recovery of the effective parameters.

corresponding to the times required to traverse the specimen by fast and slow waves, respectively,

$$\mathcal{R}_{\text{Total}} = \frac{1}{2c_0} \frac{A_{3,00} + A_{3,02}e_2^2 + A_{3,11}e_1e_2 + A_{3,20}e_1^2 + A_{3,22}e_1^2e_2^2}{\sum_{m,n=0}^{2} B_{mn}e_1^m e_2^n} \tag{14}$$

$$\mathcal{T}_{\text{Total}} = \frac{1}{c_0} \frac{A_{8,01}e_2 + A_{8,10}e_1 + A_{8,12}e_1e_2^2 + A_{8,21}e_1^2e_2}{\sum_{m,n=0}^{2} B_{mn}e_1^m e_2^n}.$$

These kernels are constant multiples of the reflection and transmission kernels given in [Fellah *et al.* , 2004] and [Sebaa *et al.* , 2006]. The coefficients are complicated functions of the parameters P, Q, R, β and the eigenvectors (5). Figure 5 shows the simulated pressure measurements $p_R(x_R, t)$ to the right of the bone.

5 Difficulty in recovering the Biot parameters

Some of the Biot-JKD parameters can be found in the literature, if the constituent materials of the frame and fluid are known. Others require observations involving the particular specimen. One approach to recovering these Biot parameters from observed pressure in a waveform p^{Obs} such as the ones illustrated in Figure 5 is to minimize difference of p^{Obs} with waveforms p^{Trial} calculated from a trial set of Biot parameters using some minimization routine such as the

	β	α_∞	Λ	K_b	G
min	0.5	1	$1\,\mu$m	5×10^8 Pa	1×10^8 Pa
max	0.99	2	$200\,\mu$m	5×10^9 Pa	5×10^9 Pa
Scale	1	1	$10\,\mu$m	10^9 Pa	10^9 Pa

Table 3: Parameter ranges for five JKD parameters.

Nelder-Mead simplex method. The difficulty with this approach is that there are typically numerous local minima, with the consequence that the result may not be near the actual parameter values unless a very good initial guess is available [Buchanan *et al.* , 2002],[Buchanan *et al.* , 2004],[Buchanan & Gilbert, 2007],[Gerstoft, 1994]. Table 3 gives ranges for the five parameters in Table 1 that require observation of the particular specimen. The ranges for porosity β, asymptotic tortuosity α_∞, and viscous characteristic length Λ are taken from [Sebaa *et al.* , 2006]. The ranges for K_b and G were chosen to encompass the range of values in Table 2.

The procedure described below is used to illustrate the difficulty in recovering the five parameters of Table 3. All other parameters were given the values in Table 2. Both p_L and p_R waveforms were assumed to be observed. A set of parameters was sought that minimized the objective function

$$f_{obj} = \left\| p_L^{\text{Trial}} - p_L^{\text{Obs}} \right\|_2 + \left\| p_R^{\text{Trial}} - p_R^{\text{Obs}} \right\|_2 + \text{Penalty}, \tag{15}$$

where the norms are the vector 2-norms with the pressures computed at 1024 discrete times. A linearly increasing penalty term was used in the objective function when a trial parameter value deviated by more than 25% from the ranges of Table 3. The general form of the penalty terms used in the algorithms presented is

$$\text{Penalty} = \sum_{n=1}^{N} \left[\max(0, v_{n,\min} - v_n) + \max(0, v_n - v_{n,\max}) \right] \tag{16}$$

where v_n is the candidate value of the n^{th} variable, and the corresponding target range is $[v_{n,\min}, v_{n,\max}]$. The simplex method worked with values that were normalized by the factors in the "Scale" row of Table 3. Because of the wide range given in Table 3 and its strong influence, the viscous characteristic length was treated specially. The initial guesses generated by Algorithm 1 were used in the simplex method to minimize (15). The implementation of the Nelder-Mead algorithm used was MATLAB's *fminsearch*. The parameter set that yielded the lowest objective function value among the 48 trial sets was selected.

Algorithm 1 *Generate a series of initial guesses:*

- *Select a parameter range,* $r_{\min}$ *to* $r_{\max}$ *from Table 3*
- *For* $h = 0.3, 0.2, 0.1$

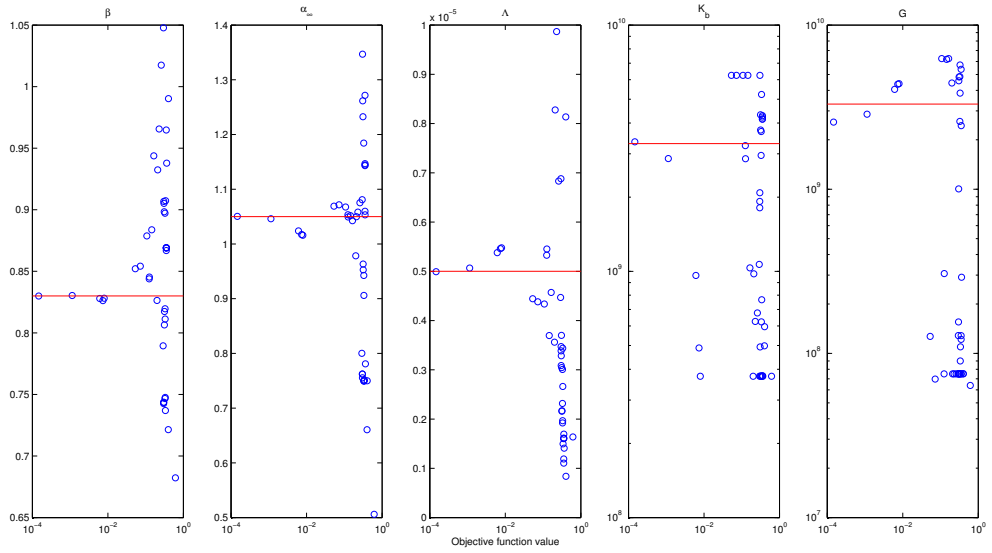

Figure 6: Outcome of Algorithm 1 vs objective function value. The specimen was M1F04. Red lines: Target values from Table 2. The specimen length was $L = 5\,\mathrm{mm}$.

- *lowvals* $= (1 + h) * r_{\min}$
- *highvals* $= (1 - h) * r_{\max}$
- *Loop through all 16 high/low combinations of* $(\beta, \alpha_\infty, K_b, G)$
  - *For each combination find the univariate minimum for* Λ *among 100 evenly spaced points between* 1 *and* $200\,\mu\mathrm{m}$.

Table 4 shows the degree of success that the simplex method with the initializations generated by Algorithm 1 had in recovering the six parameter sets of Table 2. As no noise or modelling error was present, a nearly exact recovery was possible, but this happened in only one, Sample M1F04, of the six attempts. Figures 6, 7 and 8 illustrate the presence of numerous local minima of the objective function in the cases of M1F04, M2F04, and M1S06D. Even though the stopping criteria of MATLAB's *fminsearch* were met in almost all instances, indicating that the result was likely a local minimum, more than 40 of the 48 trials in each of the six samples considered found local minima that differed from all others by 5% in at least one of the five parameter values. Even if a disagreement of at least 5% was required in one of the three most strongly influential parameters β, α_∞, and Λ, there were still typically about 20 distinct minima.

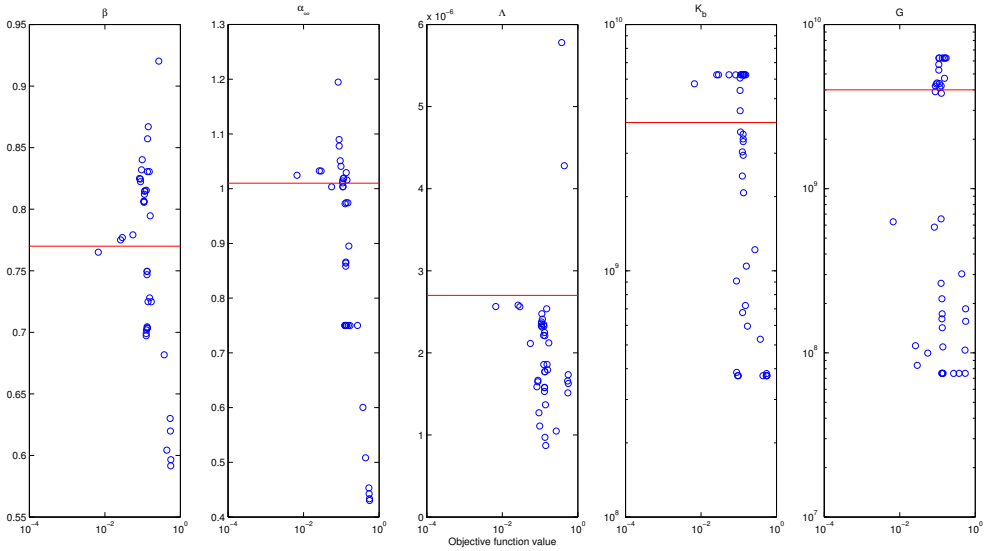

Figure 7: Outcome of Algorithm 1 vs objective function value. The specimen was M2F04. Red lines: Target values from Table 2. The specimen length was $L = 5\,\mathrm{mm}$.

Sample	β	α_∞	K_b	G	Λ	Trial #	Obj. ftn.	Time(s)
M1F04	0.830	1.050	3.36E+09	2.57E+09	4.99E-06	12	0.0001	767
Target	0.830	1.050	3.30E+09	2.60E+09	5.00E-06			
M2F04	0.765	1.025	5.74E+09	6.29E+08	2.57E-06	28	0.0067	709
Target	0.770	1.010	4.00E+09	1.70E+09	2.70E-06			
M3F04	0.879	1.023	1.51E+09	2.18E+08	4.91E-06	25	0.0013	690
Target	0.880	1.020	1.30E+09	3.50E+08	5.00E-06			
M1S06D	0.689	1.046	6.25E+09	4.53E+08	9.08E-06	19	0.0672	774
Target	0.710	1.020	4.08E+09	1.77E+09	1.04E-05			
M2S06D	0.719	1.101	2.94E+09	3.62E+08	1.29E-05	3	0.0323	841
Target	0.750	1.045	1.54E+09	9.68E+08	1.50E-05			
M3S06D	0.582	1.597	3.64E+09	7.49E+07	5.88E-06	3	0.8281	1355
Target	0.550	1.080	1.49E+09	1.07E+09	1.95E-05			

Table 4: Result of using the simplex method with each of the 48 initial guesses generated by Algorithm 1. Trial # is the initial guess that produced the lowest objective function value.

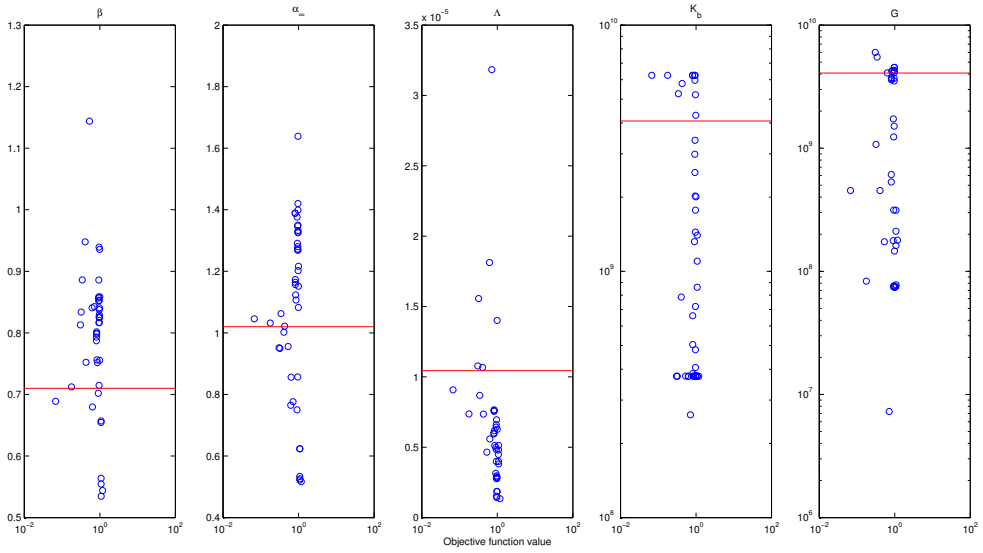

Figure 8: Outcome of Algorithm 1 vs objective function value. The specimen was M1S06D. Red lines: Target values from Table 2. The specimen length was $L = 5\,\mathrm{mm}$.

6 Effective parameters

The wave speeds and attenuations shown in Figure 3 are computable from the Biot parameters, but given the difficulties in finding these parameters directly from observed waveforms illustrated in the last section, the possibility of finding the wave speeds and attenuations directly from the observed waveforms was contemplated. The approach was based on the formulas derived in [Buchanan *et al.* , 2011a] for kernels $\mathcal{T}(\mathcal{F}_L|\mathcal{B}, J), \mathcal{T}(\mathcal{B}|\mathcal{F}_R, J), J = F, S$, and $\mathcal{R}(\mathcal{F}_L|\mathcal{B})$ representing the transmission coefficients from the fluid on the left side into the bone as a fast or slow wave, the transmission coefficient of a fast or slow wave from bone into the fluid on the right side, and reflection coefficient of a wave in the water off the left edge of the bone specimen. Recovery of the real and imaginary parts of the complex wave speeds $c_J, J = F, S$, the reflection coefficient $\mathcal{R}(\mathcal{F}_L|\mathcal{B})$ and the composite coefficients for direct (unreflected) transmission through the bone

$$\mathcal{T}_J = \mathcal{T}(\mathcal{F}_L|\mathcal{B}, J)\mathcal{T}(\mathcal{B}|\mathcal{F}_R, J), J = F, S, \tag{17}$$

was attempted at five frequencies in the range $0.5 - 4\,\mathrm{MHz}$. The magnitude and phase of the coefficients $\mathcal{T}_J$ and $\mathcal{R}(\mathcal{F}_L|\mathcal{B})$ are plotted in Figure 9. In the process of seeking frequency dependent velocities the anomaly shown in Figure 10 was encountered. The recovered speeds, represented by $\circ$ in the figure, lay on curves

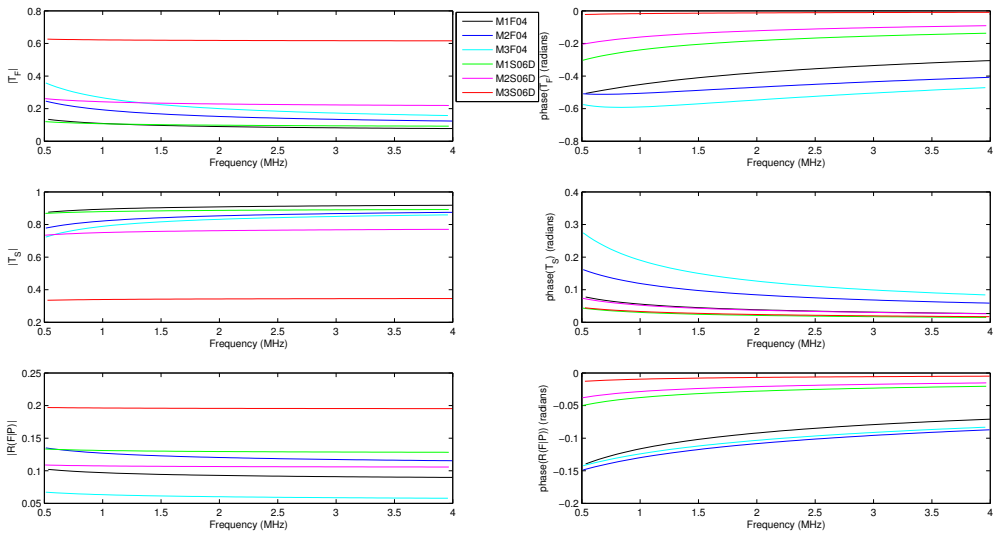

Figure 9: Top panes: Amplitude and phase of the transmission kernel $\mathcal{T}_F$. Center panes: Amplitude and phase of the transmission kernel $\mathcal{T}_S$. Bottom panes: Amplitude and phase of the reflection kernel $\mathcal{R}(\mathcal{F}_L|\mathcal{B})$(labeled as $R(F|P)$ in the graph). The formula for the kernels are given in [Buchanan *et al.* , 2011a].

different from the velocity curves of Eqn (7). The dashed-line curves in Figure 10 will be termed the *effective*, as opposed to the *intrinsic,* velocities. The formula for the effective velocity is obtained by starting with the representation for the direct arrivals of the fast and slow waves to the right of the bone and regrouping factors so that the complex-valued quantities $\mathcal{T}_J$ and c_J defined in (17) and (6) are replaced by real-valued quantities. Let the transmission coefficients $\mathcal{T}_J$ have polar representations $\mathcal{T}_J = |\mathcal{T}_J| \exp(i\varphi_J), J = F, S$. The procedure just described leads to

$$p_J(x,t) = \frac{1}{2c_0}\mathcal{L}^{-1}\left\{\mathcal{T}_J \exp\left(-s\left|x_T\right|/c_0\right)\exp\left(-sL/c_J\right)\exp\left(-s\left(x_R-L\right)/c_0\right)\frac{\hat{f}(s)}{s}\right\}$$

$$= \frac{1}{2c_0}\mathcal{L}^{-1}\left\{\begin{array}{c} |\mathcal{T}_J|\exp(i\varphi_J)\exp\left(-i\omega\frac{L}{|c_J|^2}\left(\operatorname{Re} c_J - i\operatorname{Im} c_J\right)\right)\exp\left(-i\omega\left|x_T\right|/c_0\right) \\ \exp\left(-i\omega\left(x_R-L\right)/c_0\right)\frac{\hat{f}(i\omega)}{i\omega}\end{array}\right\}$$

where as noted earlier $s = i\omega$. Define the effective transmission coefficients to be

$$\mathcal{T}'_J := |\mathcal{T}_J|\exp\left(-\omega\frac{L}{|c_J|^2}\operatorname{Im} c_J\right) = |\mathcal{T}_J|\exp\left(-\omega a_J L\right)$$

from (7), and the effective velocities to be

$$v'_J = v_J\left(1-\frac{v_J\varphi_J}{\omega L}\right)^{-1}, J = F, S. \tag{18}$$

In terms of these effective parameters, $p_J(x,t)$, $J = F, S$ can be expressed as

$$\frac{1}{2c_0}\mathcal{L}^{-1}\left\{\mathcal{T}'_J\exp\left(-i\omega\left|x_T\right|/c_0\right)\exp\left(-i\omega L/v'_J\right)\exp\left(-i\omega\left(x_R-L\right)/c_0\right)\frac{\hat{f}(i\omega)}{i\omega}\right\} \tag{19}$$

As indicated in Figure 10 the effective velocity curves better track the recovered velocities. Figure 11 shows the intrinsic and effective wave speeds for the six samples of Table 2. Similarly, if $\mathcal{R}(\mathcal{F}_L|\mathcal{B}) = \mathcal{R}_0\exp(i\theta)$, then the effective velocity of the reflected wave is found to be

$$c'_0 = c_0\left(1-\frac{\theta c_0}{\omega\left|x_T\right|}\right)^{-1}.$$

Algorithms 2 and 3 generate initial estimates to be used in the simplex method to obtain frequency-independent estimates for $v'_J, \mathcal{T}'_J, J = F, S, \mathcal{R}_0, c'_0$. Since the coefficients $\mathcal{T}'_J$ and $\mathcal{R}_0$ are expected to be between 0 and 1, they can be found by a fairly coarse sweep of this interval. The effective velocities v'_J can be estimated from observation of the transmitted wave form, thereby narrowing

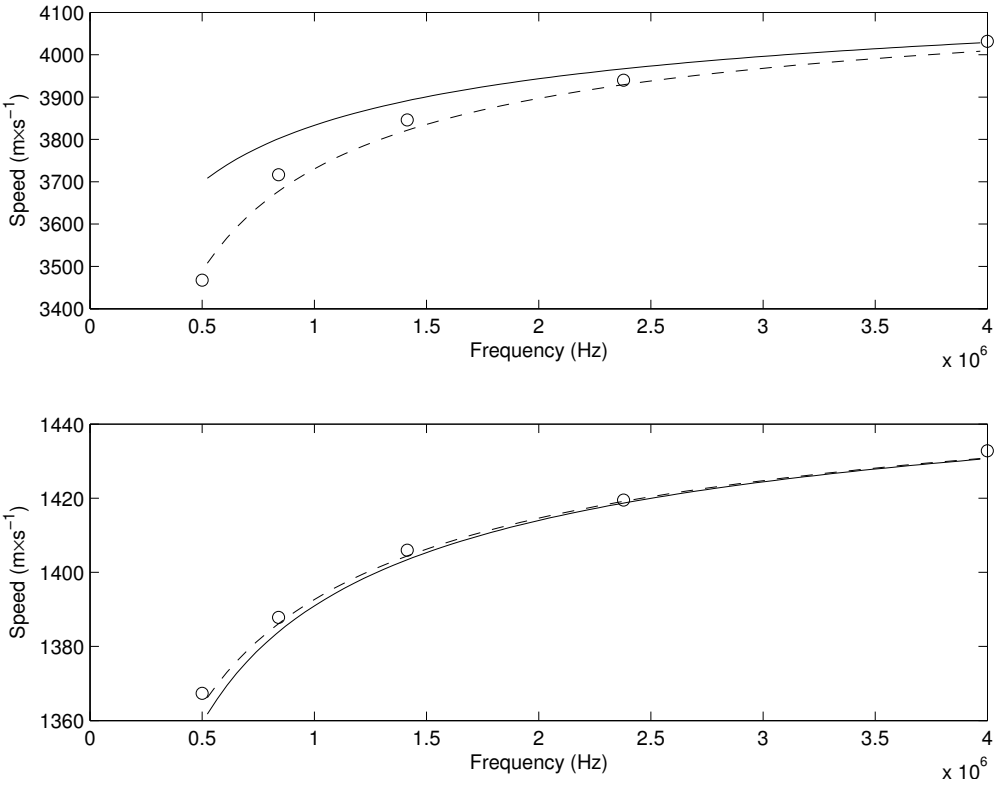

Figure 10: A preliminary attempt to recover the intrinsic wave speeds v_J in (7) [solid line] from observed waveforms led instead to recovery of the effective wave speeds v'_J in (18) [dashed line]. Top: $J = F$. Bottom: $J = S$. The sample was M1F04 and the length was $L = 5\,\mathrm{mm}$.

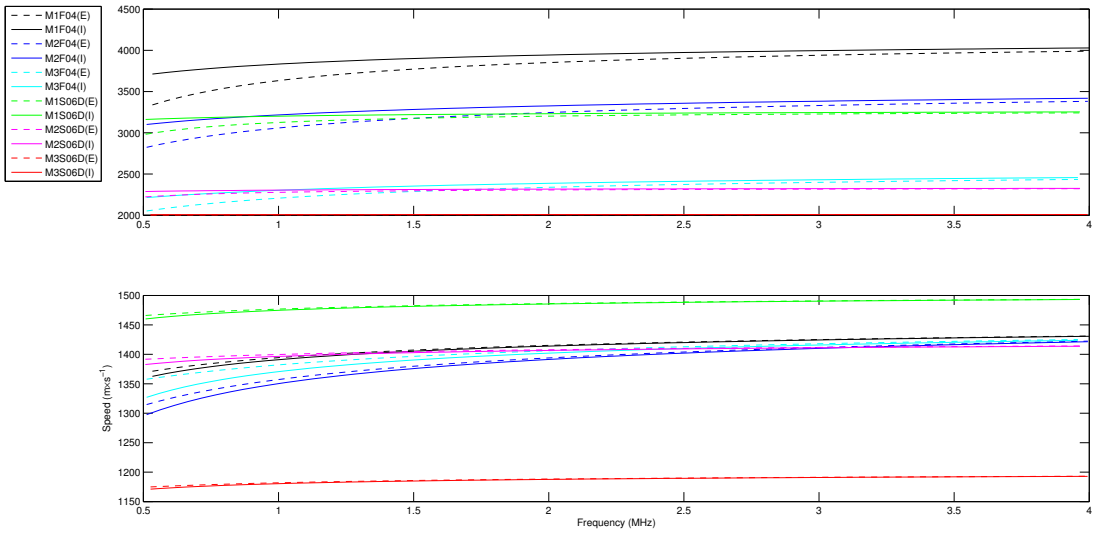

Figure 11: Solid lines are the intrinsic velocities $v_J, J = F, S$. Dashed lines are the effective velocities v'_J. Top: $J = F$. Bottom: $J = S$

	v'_F	T'_F	v'_S	T'_S
min	$1900\,\mathrm{m}\cdot\mathrm{s}^{-1}$	0	$950\,\mathrm{m}\cdot\mathrm{s}^{-1}$	0
max	$4100\,\mathrm{m}\cdot\mathrm{s}^{-1}$	1	$1550\,\mathrm{m}\cdot\mathrm{s}^{-1}$	1
Scale	$10^3\,\mathrm{m}\cdot\mathrm{s}^{-1}$	10^{-1}	$10^3\,\mathrm{m}\cdot\mathrm{s}^{-1}$	10^{-1}

Table 5: Parameter ranges for four transmitted effective parameters.

the range of guesses required. The trial pressures

$$p_R^{\mathrm{Trial}} = \frac{1}{2c_0}\mathcal{L}^{-1}\left\{ \begin{array}{c} \left(\mathcal{T}'_F \exp\left(-sL/v'_F\right) + \mathcal{T}'_S \exp\left(-sL/v'_S\right)\right) \\ \exp\left(-st_W\right)\frac{\hat{f}(s)}{s} \end{array} \right\} \tag{20}$$

$$p_L^{\mathrm{Trial}} = \frac{1}{2c_0}\mathcal{L}^{-1}\left\{ \mathcal{R}_0 \exp\left(-s\left|x_T\right|/c'_0\right)\exp\left(-s\left|x_T\right|/c_0\right)\frac{\hat{f}(s)}{s} \right\}$$

for the direct transmitted and reflected arrivals were used in (15). A penalty term of the form (16) was imposed if T'_F, v'_F, T'_S or v'_S moved outside of the ranges shown in Table 5.

Algorithm 2 *Generate initial estimates for transmitted effective parameters:*

- *Obtain approximate arrival times t_{F0} and t_{S0} for the fast and slow waves by observation (Figure 5)*

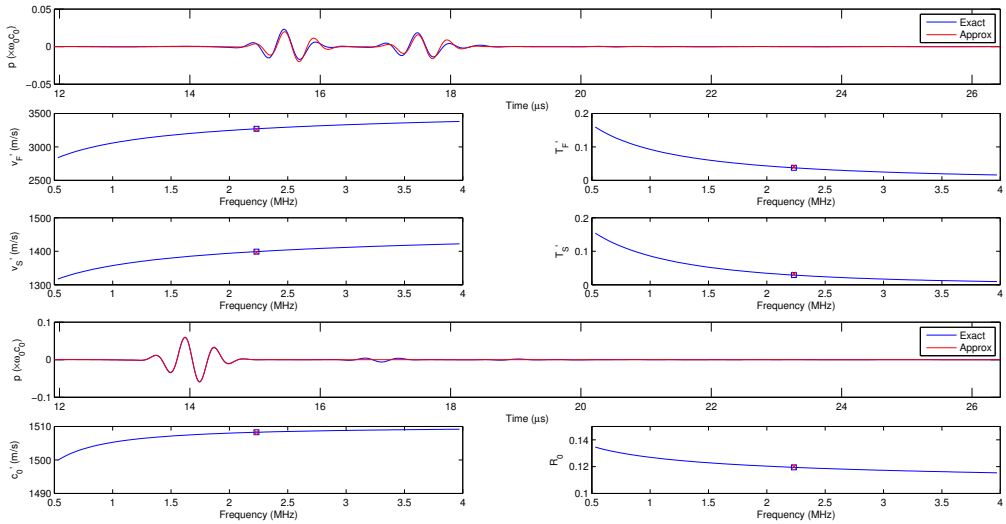

Figure 12: First row: Exact and approximate transmitted waveforms. Fifth row: Exact and approximate reflected waveforms. Remaining panels: Blue square: actual value of effective quantity; red x: inversion value of effective parameters at frequency 2.24 MHz The specimen was M2F04 and the length $L = 5\,\text{mm}$.

- *For* $m = 0, \ldots, M, J = F, S$ *calculate times* $t_{Jm} = t_{J0} + m \times 0.025 \times 10^{-5}\,\text{s}$
  - *Estimate trial wave speeds* $v'_J = L/\left(t_{Jm} - t_W\right)$
  - *For* $n = 1, \ldots, N$ *estimate* $\mathcal{T}'_F = \mathcal{T}'_S = 1 - n/N$

In the above t_W is the time that the pulse travels through water, i.e. $t_W = \frac{|x_T| + x_R - L}{c_0}$. The algorithm for generating estimates for $\mathcal{R}_0$ and c'_0 was

Algorithm 3 *Generate the initial estimates for reflected effective parameters:*

- $c'_0 = c_0$
- *For* $n = 1, \ldots, 5$
  - $\mathcal{R}_0 = 1.1 - 0.2n$

Figures 12 and 13 illustrate the outcomes of applying Algorithms 2 and 3 for the two samples M2F04 and M2S06D. The constant approximations to the six parameters are all seen to be near the correct values at the center frequency. Table 6 gives the results for all six samples of Table 2. Typically the values of the effective parameters given in Table 6 were the best of a small number of

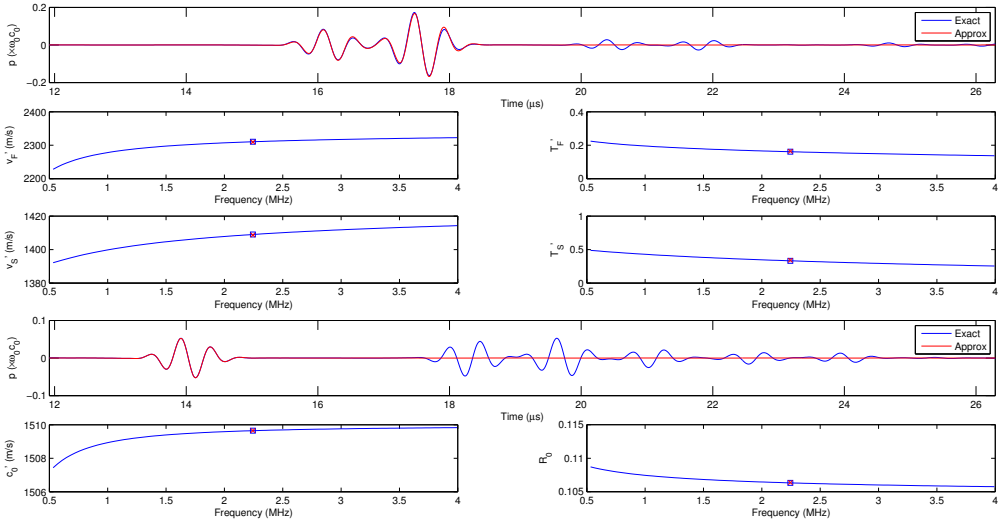

Figure 13: First row: Exact and approximate transmitted waveforms. Fifth row: Exact and approximate reflected waveforms. Remaining panels: Blue square: actual value of effective quantity; red x: inversion value of effective at frequency 2.24 MHz The specimen was M2S06D and the length $L = 5\,\text{mm}$. As can be seen the trial pressures attempted only to approximate the directly transmitted and reflected arrivals.

	v'_F	v'_S	c'_0	$\mathcal{T}'_F$	$\mathcal{T}'_S$	$\mathcal{R}_0$
M1F04	3868	1418	1508.5	0.034	0.146	0.093
Actual	3880	1418	1508.5	0.032	0.141	0.092
M2F04	3259	1397	1508.2	0.040	0.032	0.120
Actual	3271	1399	1508.3	0.037	0.029	0.119
M3F04	2346	1408	1508.3	0.029	0.059	0.060
Actual	2357	1410	1508.4	0.026	0.055	0.060
M1S06D	3208	1487	1509.5	0.065	0.412	0.129
Actual	3209	1487	1509.5	0.064	0.404	0.129
M2S06D	2310	1409	1509.7	0.164	0.340	0.106
Actual	2310	1409	1509.7	0.161	0.332	0.106
M3S06D	2008	1189	1509.7	0.605	0.155	0.196
Actual	2008	1189	1509.9	0.605	0.151	0.196

Table 6: Recovery of constant approximations to the effective parameters for six samples. The values labeled "Actual" are those at the center frequency.

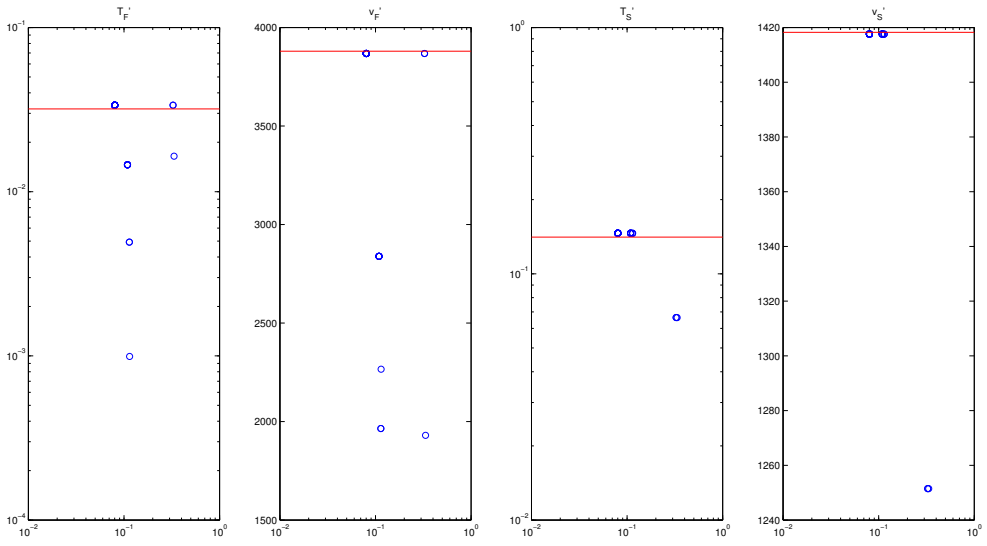

Figure 14: Physically reasonable local minima of the effective parameters found by Algorithm 2 with $M = 2, N = 20$. The horizontal axis is the value of the objective function. Red line: Target value. The sample was M1F04.

physically reasonable (as defined by Table 5) local minima. Figure 14 illustrates this.

The effective velocities and kernels have the undesirable trait of depending upon the length L of the specimen. Recovery of the intrinsic velocities and kernels could be accomplished by computing the effective parameters at two different lengths L_1 and L_2 by means of the formulae

$$\begin{aligned} a_J &= -\frac{1}{\omega\left(L_1 - L_2\right)} \log\left(\frac{\mathcal{T}'_{J1}}{\mathcal{T}'_{J2}}\right) \\ |\mathcal{T}_J| &= \mathcal{T}'_{Jm} \exp\left(\omega a_J L_m\right), m = 1, 2 \\ v_J \varphi_J &= \frac{L_1 L_2 \omega \left(v'_{J2} - v'_{J1}\right)}{L_1 v'_{J2} - L_2 v'_{J1}} \\ v_J &= v'_{Jm}\left(1 - \frac{v_J \varphi_J}{\omega L_m}\right), m = 1, 2, \end{aligned} \tag{21}$$

however this may not be necessary as accurate approximation of the effective parameters by the approach described in the next section may permit recovery of the original Biot parameters.

7 A new approach for recovering the Biot parameters

Denote the numerical approximation to an effective parameter at the center frequency found by Algorithm 2 or 3 with a tilde, e.g. $\tilde{v}'_F(\omega_0)$. The equations for calculating the effective parameters

$$\begin{aligned} v'_F(\omega_0, \beta, \alpha_\infty, \Lambda, K_b, G) &= \tilde{v}'_F(\omega_0) \\ v'_S(\omega_0, \beta, \alpha_\infty, \Lambda, K_b, G) &= \tilde{v}'_S(\omega_0) \\ \mathcal{T}'_F(\omega_0 \beta, \alpha_\infty, \Lambda, K_b, G) &= \tilde{\mathcal{T}}'_F(\omega_0) \\ \mathcal{T}'_S(\omega_0, \beta, \alpha_\infty, \Lambda, K_b, G) &= \tilde{\mathcal{T}}'_S(\omega_0) \\ R_0(\omega_0, , \beta, \alpha_\infty, \Lambda, K_b, G) &= \tilde{\mathcal{R}}_0(\omega_0) \end{aligned} \tag{22}$$

constitute five equations in the five unknown Biot parameters. The system of equations may be solved by Newton's method, for instance. The details are given in Algorithm 4.

Algorithm 4 *Find the Biot parameters by solving the system of nonlinear equations (22):*

- *Find* $\tilde{v}'_F(\omega_0), \tilde{v}'_S(\omega_0), \tilde{\mathcal{T}}'_F(\omega_0), \tilde{\mathcal{T}}'_S(\omega_0), \tilde{\mathcal{R}}_0(\omega_0)$ *using Algorithms 2 and 3*
- *For* $h = 0.45, 0.37, 0.29, \ldots, 0.05$
  - *lowvals* $= (1 + h) * [.5, 1, 1e8, 1e8, 1e - 6]$

Sample		β	α_∞	Λ	K_b	G	Try #	Obj. ftn.	Time(s)
M1F04	Newt	0.827846	1.04542	5.31E-06	2.49E+09	3.10E+09	15		
	Simp	0.830006	1.04281	5.12E-06	2.56E+09	3.06E+09		0.0019	20.618
	Targ	0.83	1.05	5.00E-06	3.30E+09	2.60E+09			
M2F04	Newt	0.768722	1.01787	2.85E-06	3.88E+09	1.75E+09	14		
	Simp	0.770182	1.00765	2.71E-06	3.79E+09	1.83E+09		0.0008	22.238
	Targ	0.77	1.01	2.70E-06	4.00E+09	1.70E+09			
M3F04	Newt	0.878734	1.0214	5.33E-06	1.15E+09	4.32E+08	47		
	Simp	0.880555	1.01708	5.08E-06	1.11E+09	4.72E+08		0.0012	28.815
	Targ	0.88	1.02	5.00E-06	1.30E+09	3.50E+08			
M1S06D	Newt	0.709967	1.02027	1.10E-05	3.99E+09	1.82E+09	11		
	Simp	0.711586	1.01754	1.05E-05	3.95E+09	1.84E+09		0.0016	21.945
	Targ	0.71	1.02	1.04E-05	4.08E+09	1.77E+09			
M2S06D	Newt	0.749729	1.04305	1.57E-05	1.49E+09	9.96E+08	3		
	Simp	0.751109	1.04221	1.51E-05	1.48E+09	9.94E+08		0.0012	14.695
	Targ	0.75	1.045	1.50E-05	1.54E+09	9.68E+08			
M3S06D	Newt	0.550511	1.07425	2.05E-05	1.43E+09	1.09E+09	19		
	Simp	0.550208	1.07387	1.96E-05	1.44E+09	1.09E+09		0.0032	29.043
	Targ	0.55	1.08	1.95E-05	1.49E+09	1.07E+09			

Table 7: Application of Algorithm 4 for a specimen width of $L = 5$mm . In Algorithm 2 $M = 2, N = 20$.

  - *highvals* $= (1-h) * [.99, 2, 1e10, 1e10, 200e-6]$
  - *Loop through all 16 high/low combinations of the first four parameters* $(\beta, \alpha_\infty, K_b, G)$
    * *For each combination find approximate value for* Λ *by solving* $\mathcal{T}'_S(\omega_0, \beta, \alpha_\infty, \Lambda, K_b, G) = \hat{\mathcal{T}}'_S(\omega_0)$. *Use half and twice this value as the low/high for* Λ
    * *Use* $(\beta, \alpha_\infty, \Lambda, K_b, G)$ *as an initial guess in Newton's method*
    * *If it converges to physically reasonable values (Table 3) stop.*

- *Use the result as an initialization in simplex method (*MATLAB *fminsearch)*

Table 7 shows the result of applying Algorithm 4 to find the parameters of Table 2 for a specimen length of $L = 5\,\text{mm}$.

A difficulty in assessing parameter recovery schemes is that, in the absence of actual experimental data, simulated experimental data must be used. Ideally there exist two independent computational procedures which are known to agree well with experimental observation so that one can be used for the simulated experimental data and the other to generate the trial parameter data. In the present case the Biot-JKD model has produced by far the best agreement with experimental observation and so it is used for both the simulated experimental data and the trial data. This may result in the proposed recovery algorithm

producing unrealistically accurate results since modeling error, the discrepancy between the experimental observations and the best-fit trial solution, is not present. An instance of this was noted in connection with Algorithm 1 in the case of M1F04 (Table 4).

Figure 15 shows the effect of varying the parameter t_c in formula (11) on the reflected and transmitted waveforms in the case of sample M2F04. Figures 16 and 17 show the outcome of Algorithms 2 and 3 when $t_c = 2.0t_0$ is used for the simulated experimental waveforms while $t_c = 1.75t_0$ is used in computing trial parameter sets (cf Figures 12 and 13). Since the effect is reminiscent of the discrepancies observed in [Sebaa *et al.* , 2006], Figures 15-17, the robustness of Algorithm 4 will be assessed by using $t_c = 1.75t_0$ for computing trial waveforms, but using some other value t_c^{Obs} for the simulated experimental waveform. It was found that Algorithm 4 in the form presented above sufficed for $t_c^{\text{Obs}} = 1.8t_0$ and $1.9t_0$. For $t_c^{\text{Obs}} = 2.0t_0$ there was still a local minimum of the objective function that corresponded to a good approximation to the effective parameters, but it was not necessarily the global minimum. Moreover even for the most accurate set of effective parameters the recovered parameters did not necessarily correspond to a fully plausible solution, since while typically β and Λ were plausible, one of K_b or G were negative, or, and sometimes additionally, $\alpha_\infty < 1$. The following modification of Algorithm 4 was used. It uses the effective parameters which correspond to the three lowest objective function values, rather than just the lowest one.

Algorithm 5 *Find Biot parameters in the event of trial/experimental data discrepancies*

- *Find the sets of distinct effective parameters* $\tilde{v}'_{Fj}(\omega_0), \tilde{v}'_{Sj}(\omega_0), \tilde{\mathcal{T}}'_{Fj}(\omega_0), \tilde{\mathcal{T}}'_{Sj}(\omega_0), j = 1, 2, 3$ *with lowest objective function values using Algorithm 3*
- *Find* $\tilde{\mathcal{R}}_0(\omega_0)$ *using Algorithm 3*
- *For* $j = 1, 2, 3$ *using* $\tilde{v}'_{Fj}(\omega_0), \tilde{v}'_{Sj}(\omega_0), \tilde{\mathcal{T}}'_{Fj}(\omega_0), \tilde{\mathcal{T}}'_{Sj}(\omega_0)$
  - *For* $h = 0.05 + 0.08k$, $k = 0$ *to* 5.
    - *lowvals* $= (1 + h) * [.5, 1, 1e8, 1e8, 1e - 6]$
    - *highvals* $= (1 - h) * [.99, 2, 1e10, 1e10, 200e - 6]$
    - *Loop through all 16 high/low combinations of the first four parameters* $(\beta, \alpha_\infty, K_b, G)$
    - *For each combination find approximate value for* Λ *by solving* $\mathcal{T}'_S(\omega_0, \beta, \alpha_\infty, \Lambda, K_b, G) = \hat{\mathcal{T}}'_{Sj}(\omega_0)$ *use half and twice this value as the low/high for* Λ
    - *Use* $(\beta, \alpha_\infty, \Lambda, K_b, G)$ *as an initial guess in Newton's method. If it converges to physically reasonable values (Table 3) terminate both* h *and* j *loops*
- *If the* j *loop terminated with a physically reasonable value, use the result as an initialization in simplex method (*MATLAB *fminsearch)*

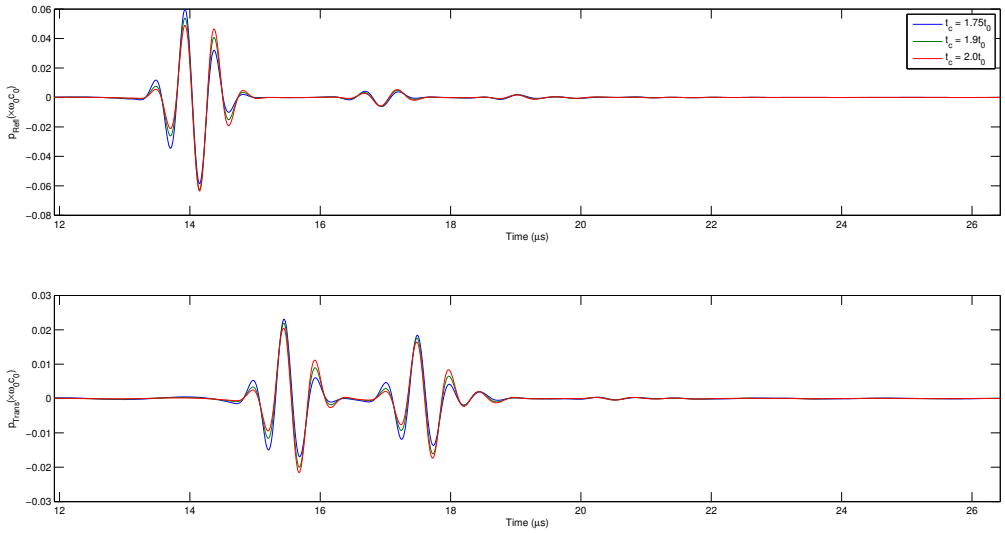

Figure 15: Effect of varying the parameter t_c on the transmitted wave form. The sample was M2F04 and the specimen length was $L = 5\,\text{mm}$.

- *Otherwise if the j loop terminates with one or more parameter sets that are not completely physically reasonable*
  - *For the parameter set with lowest objective function value*
    - *Reset any unreasonable value to the proximate reasonable value of Table 3*
    - *Use the result as an initialization in simplex method (*MATLAB *fminsearch)*

Table 8 shows the result of applying Algorithm 5 with $t_c = 2.0t_0$ used for the simulated experimental observations. For two of the samples no completely reasonable parameter set was found, but sending the amended results to the simplex method did produce a physically plausible result. Whether the Newton phase terminated successfully or not did not affect the final objective function value discernibly. Table 9 shows the effect of the increasing discrepancy in t_c for the trial and simulated experimental waveforms up to $t_c = 2.2t_0$ where Algorithm 5 experienced its first failure. Up through $t_c = 2.0t_0$ the errors tended to increase monotonically and the deterioration did not markedly correlate with whether the Newton phase of the algorithm produced a fully physically reasonable answer or not. For $t_c = 2.1t_0$ and $2.2t_0$ the results became more idiosyncratic. For instance for M1F04 the algorithm terminated successfully with an accurate answer after the Newton phase for $t_c = 2.2t_0$, but not for $t_c = 2.0t_0$

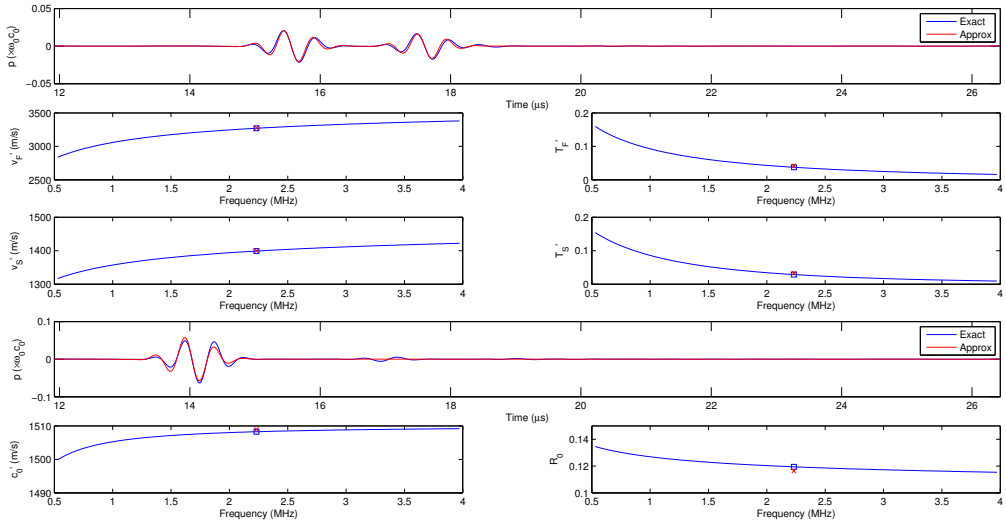

Figure 16: Outcome of Algorithms 2 and 3 when in (11) $t_c = 1.75t_0$ is used for trial solutions, but $t_c = 2.0t_0$ is used for the simulated experimental observation. The sample is M2F04 of Table 2, the specimen length is $L = 5\,\mathrm{mm}$.

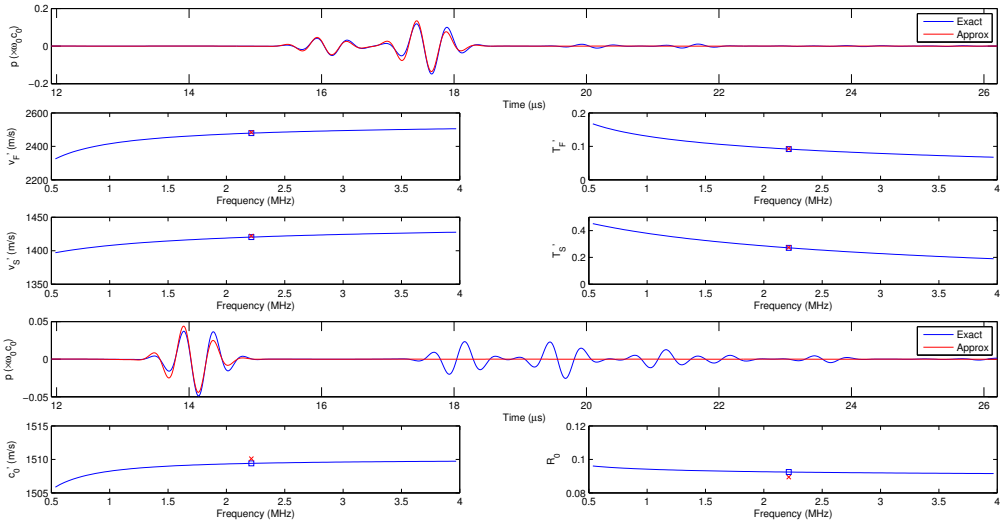

Figure 17: Outcome of Algorithms 2 and 3 when in (11) $t_c = 1.75t_0$ is used for trial solutions, but $t_c = 2.0t_0$ is used for the simulated experimental observation. The sample is M2S06 of Table 2, the specimen length is $L = 5\,\mathrm{mm}$.

Sample		β	α_∞	Λ	K_b	G	Try #	Obj. ftn.	Time(s)
M1F04	Newt	0.817361	0.994453	5.88E-06	-9.04E+08*	5.29E+09	577*		
	Simp	0.826142	1.00661	5.45E-06	1.22E+08	4.56E+09		0.14	176
	Targ	0.83	1.05	5.00E-06	3.30E+09	2.60E+09			
M2F04	Newt	0.771267	0.982397	3.13E-06	1.26E+09	3.35E+09	14		
	Simp	0.772825	0.983964	2.87E-06	2.18E+09	2.84E+09		0.10	25
	Targ	0.77	1.01	2.70E-06	4.00E+09	1.70E+09			
M3F04	Newt	0.879108	0.994889	6.01E-06	-1.73E+08*	1.29E+09	577*		
	Simp	0.881484	0.996204	5.46E-06	1.23E+08	1.12E+09		0.07	157
	Targ	0.88	1.02	5.00E-06	1.30E+09	3.50E+08			
M1S06D	Newt	0.718138	0.994846	1.13E-05	3.02E+09	2.31E+09	11		
	Simp	0.718306	0.992291	1.09E-05	3.01E+09	2.31E+09		0.31	19
	Targ	0.71	1.02	1.04E-05	4.08E+09	1.77E+09			
M2S06D	Newt	0.755936	1.0233	1.58E-05	1.12E+09	1.16E+09	3		
	Simp	0.755056	1.02191	1.55E-05	1.13E+09	1.16E+09		0.30	15
	Targ	0.75	1.045	1.50E-05	1.54E+09	9.68E+08			
M3S06D	Newt	0.569176	1.11516	1.85E-05	1.58E+09	1.01E+09	19		
	Simp	0.564775	1.11435	1.89E-05	1.62E+09	9.95E+08		0.72	35
	Targ	0.55	1.08	1.95E-05	1.49E+09	1.07E+09			

Table 8: Application of Algorithm 5 for a specimen length of $L = 5$mm . In Algorithm 2 $M = 2, N = 20$. *: For M1F04 and M3F04 the algorithm ran through three effective parameter sets without finding a completely reasonable solution.

and $t_c = 2.1t_0$ where the last stage of the algorithm had to be invoked and the answers were less accurate. This suggests that Algorithm 2 failed to find the global minimum for the last-mentioned values of t_c, but a more exhaustive search failed to confirm this. Also between $t_c = 2.1t_0$ and $t_c = 2.2t_0$ the errors were less likely to decline.

8 Summary and Conclusions

This article affirms that the well-known difficulty with parameter recovery schemes based on minimization, the presence of numerous local minima, obtains in the case of recovering the parameters of the Biot-JKD model. A different approach, based upon numerical solution of the equations for a set of five effective wave speeds and transmission and reflection coefficients, seems promising. While the first stage of the proposed algorithm, recovery of the effective parameters, does admit multiple solutions, the availability of good guesses for the effective wave speeds, and the narrow range for the reflection and transmission coefficients, makes determination of the probable global minimum easier. The second stage of the algorithm, numerical solution of the system of equations, appears to have few solutions, with no more than one physically plausible solution being detected in any simulation done thus far. This second stage of the proposed

Sample	T_c	β	α_∞	Λ	K_b	G
M1F04	1.8	0.13%	1.22%	3.78%	35.13%	28.24%
	1.9	0.42%	2.93%	7.65%	73.80%	58.89%
	2*	0.46%	4.13%	9.07%	96.29%	75.29%
	2.1*	5.15%	3.15%	7.10%	97.73%	288.26%
	2.2	1.32%	3.24%	0.84%	66.80%	43.31%
M2F04	1.8	0.01%	0.55%	1.66%	10.80%	16.47%
	1.9	0.05%	1.27%	3.48%	22.35%	34.13%
	2	0.37%	2.58%	6.47%	45.56%	66.87%
	2.1*	0.44%	5.79%	13.47%	97.13%	138.97%
	2.2*	1.25%	5.85%	12.48%	96.82%	135.36%
M3F04	1.8	0.04%	0.66%	3.17%	28.60%	69.24%
	1.9	0.06%	1.57%	6.80%	63.28%	153.64%
	2*	0.17%	2.33%	9.15%	90.56%	219.03%
	2.1*	0.40%	2.48%	7.57%	92.06%	221.67%
	2.2	Failed				
M1S06D	1.8	0.06%	0.15%	0.56%	1.12%	1.38%
	1.9	0.59%	1.23%	2.97%	12.21%	14.49%
	2	1.17%	2.72%	4.70%	26.11%	30.40%
	2.1	1.58%	3.33%	2.48%	30.41%	33.96%
	2.2*	1.68%	7.92%	7.24%	66.05%	76.38%
M2S06D	1.8	0.10%	0.55%	1.49%	6.64%	5.18%
	1.9	0.18%	1.26%	2.43%	14.33%	11.30%
	2	0.67%	2.21%	3.43%	26.75%	19.55%
	2.1	1.07%	3.46%	3.20%	41.31%	29.81%
	2.2	0.37%	0.35%	9.64%	9.82%	9.30%
M3S06D	1.8	0.12%	0.57%	1.04%	3.66%	2.14%
	1.9	1.23%	0.38%	0.35%	2.10%	0.56%
	2	2.69%	3.18%	2.94%	8.98%	7.06%
	2.1	4.84%	6.09%	8.55%	18.80%	14.86%
	2.2	8.53%	9.47%	14.81%	26.95%	23.63%

Table 9: Percentage error when the target reflected and transmitted waveforms were computed with $t_c = T_c t_0$, but the trial waveforms are computed with $t_c = 1.75 t_0$. *: no completely reasonable parameter set was found and the last part of Algorithm 5 was used. The sample length was $L = 5$mm.

approach has three possible outcomes: a fully physically reasonable solution, a partially reasonable solution or no solution. It is thus possible that the success or failure of this stage of the algorithm indicates the extent to which the poroelastic medium under consideration is accurately approximated by the isotropic Biot-JKD model.

9 Acknowledgements

This research for R. Gilbert was partially sponsored by the National Science Foundation through ARRA-NSF-DMS Grant 0920850. M-J Ou's research is partially sponsored by ARRA-NSF-DMS Grant 0920852.

References

[Biot, 1962a] Biot, M. A. 1962a. Mechanics of deformation and acoustic propagation in porous media. *J. Applied Physics*, **33**(4), 1482–1498.

[Biot, 1956a] Biot, M.A. 1956a. Theory of propagation of elastic waves in a fluid-saturated porous solid. I. Lower frequency range. *J. Acoust. Soc Am.*, **28**(2), 168–178.

[Biot, 1956b] Biot, M.A. 1956b. Theory of propagation of elastic waves in a fluid-saturated porous solid. II. Higher frequency range. *J. Acoust. Soc. Am.*, **28**(2), 179–191.

[Biot, 1962b] Biot, M.A. 1962b. Generalized theory of acoustic propagation in porous dissipative media. *J. Acoust. Soc. Am.*, **34**(5), 1254–1264.

[Buchanan & Gilbert, 2007] Buchanan, J. L., & Gilbert, R. P. 2007. Determination of the parameters of cancellous bone using high frequency acoustic measurements: II Inverse problems. *Journal of Computational Acoustics*, **15**(2), 199–220.

[Buchanan *et al.* , 2002] Buchanan, J.L., Gilbert, R.P., & Khashanah, K. 2002. Recovery of the poroelastic parameters of cancellous bone using low frequency acoustic interrogation. *Pages 41–47 of:* Wirgin, A. (ed), *Acoustics, Mechanics, and the Related Topics of Mathematical Analysis*. World Scientific.

[Buchanan *et al.* , 2004] Buchanan, J.L., Gilbert, R. P., & Khashanah, K. 2004. Determination of the parameters of cancellous bone using low frequency acoustic measurements. *J. of Computational Acoustics*, **12**(2).

[Buchanan *et al.* , 2011a] Buchanan, J.L., Gilbert, R.P., & Ou, M. 2011a. Transfer functions for a one-dimensional fluid-poroelastic system subject to an ultrasonic pulse. *Nonlinear Analysis: Real World Applications*. To appear.

[Buchanan *et al.* , 2011b] Buchanan, J.L., Gilbert, R.P., & Ou, M. 2011b. Wavelet decomposition of transmitted ultrasound wave through a 1-D muscle-bone system. *Journal of Biomechanics*, **44**(2), 352–358.

[Chotiros, 2002] Chotiros, N.P. 2002. An inversion for Biot parameters in water-saturated sands. *J. Acoust. Soc. Am.*, **112**(5), 1853–1868.

[Fellah *et al.* , 2004] Fellah, Z. E. A., Chapelon, Y., Berger, S., Lauriks, W., & Depollier, C. 2004. Ultrasonic wave propagation in human cancellous bone: Application of Biot theory. *Jour. Acoustic Soc. Amer.*, **116**, 61–73.

[Gerstoft, 1994] Gerstoft, P. 1994. Inversion of seismoacoustic data using genetic algorithms an a posteriori probability distributions. *J. Acoust. Soc. Am.*, **95**(2), 770–782.

[Haire & Langton, 1999] Haire, T.J., & Langton, C.M. 1999. Biot Theory: A Review of its Application to Ultrasound Propagation Through Cancellous Bone. *Bone*, **24**(4), 291–295.

[Hosokawa & Otani, 1997] Hosokawa, A., & Otani, T. 1997. Ultrasonic wave propagation in bovine cancellous bone. *J. Acouist. Soc. Am.*, **101**, 558–562.

[Johnson *et al.* , 1987] Johnson, D. L., Koplik, J., & Dashen, R. 1987. Theory of dynamic permeability and tortuosity in fluid-saturated porous media. *J. Fluid Mech.*, **176**, 379–402.

[McKelvie & Palmer, 1991] McKelvie, M. L., & Palmer, S. B. 1991. The interaction of ultrasound with cancellous bone. *Phys. Med. Biol.*, **10**, 1331–1340.

[Sebaa *et al.* , 2006] Sebaa, N., Fellah, Z. E. A., Fellah, M., Ogam, E., Wirgin, A., Mitri, F. G., Depollier, C., & Lauriks, W. 2006. Ultrasonic characterization of human cancellous bone using the Biot theory: Inverse problem. *The Journal of the Acoustical Society of America*, **120**, 1816–1824.